Article

Operational Reliability Assessment of an Interconnected Power System Based on an Online Updating External Network Equivalent Model with Boundary PMU

Dabo Zhang [1],*, Shuai Lian [1], Weiqing Tao [1], Jinsong Liu [2] and Chen Fang [2]

[1] School of Electrical Engineering and Automation, Hefei University of Technology, Hefei 230009, China; ls_hfut2016@163.com (S.L.); twq@csg.com.cn (W.T.)
[2] Electric Power Research Institute, State Grid Shanghai Municipal Electric Power Company, Shanghai 200437, China; liujinsong1888@126.com (J.L.); fangc02@gmail.com (C.F.)
* Correspondence: zhangdb2004@163.com

check for updates

Abstract: Information between interconnected power systems is difficult to share in real time, due to trade secrets and technical limitations. The regional power grid cannot timely detect the impact of changes in the operation mode of the external power grid on the regional reliability, due to faults, load fluctuations, power generation plan adjustments, and other reasons. How to evaluate the reliability of a regional power system under the conditions of information isolation is a difficult problem for the security of interconnected power systems. Aiming at this problem, an operational reliability evaluation method for an interconnected power system is proposed herein, which does not depend on external network information directly, but only uses boundary phasor measurement unit (PMU) measurement data and internal network information. A static equivalent model with sensitivity consistency was used to simplify the external network to ensure the accuracy of the reliability calculation of interconnected power systems. The boundary PMU measurement data were used to update the external network equivalent model online. The algorithm flow of the operation reliability assessment for the interconnected power grid is given. The results of an example based on the IEEE-RTS-96 test system show that the proposed method can track the equivalent parameters of the external network without depending on the actual topological information, and calculate the reliability index of the internal network accurately.

Keywords: interconnected power system; phasor measurement unit; operational reliability assessment; static equivalent model

1. Introduction

With the increase of global power consumption and the innovation of high-voltage transmission technology [1], there are no technical barriers for long-distance and wide-range power transmission [2,3]. The interconnection of power systems in different regions has many advantages, such as promoting the consumption of renewable energy, reducing the dependence on fossil energy, reducing environmental pollution, adjusting the peak–valley difference of load, improving the reliability of power grids, and so on. Interconnected power grids are becoming increasingly large [4], not only interconnecting power grids across regions, but also interconnecting transnational power grids and global transcontinental power grids [5,6].

While interconnected power systems bring significant benefits, they also raise many problems. Local faults can spread to the whole interconnected power system and cause serious consequences.

Faults in northern Germany can affect customers hundreds of kilometers away in France, Italy, and Spain [7]. Statistical data of blackouts worldwide from 1965 to 2015 show that, with the continuous expansion of interconnection of power systems, the number of customers affected by blackouts, the area of fault propagation, and the restoration duration are constantly increasing [8,9]. The Northeast blackout in 1965 in the United States and Canada affected 30 million people, while the Indian blackout in July 2012 affected 620 million people [10]. Large-scale interconnected power systems are composed of networks of different power companies, different regions, and even different countries. Due to business secrets and technical limitations, it is difficult for local operation data to be shared with all companies in interconnected power systems in time, which limits the ability of power companies to cope with operational risks. Especially when the risk comes from the external network, the internal network often cannot be adjusted in time. How to inspect the operation status of the external network online and to evaluate the impact on the reliability of the internal network is of great significance for the safe operation of the power system.

In order to deal with the risk of interconnected power systems, research on wide-area protection based on phasor measurement unit (PMU) is gaining more attention [11–13]. A PMU model was developed in the MODELS section of the Alternative Transients Program/The Electromagnetic Transients Program (ATP/EMTP) software platform for wide-area protection [11]. The compliance of PMU algorithms and devices for wide areas stabilizing the control of large power systems was analyzed in Reference [12]. An adaptive PMU-based wide-area backup protection scheme for power transmission lines was proposed in Reference [13]. However, these methods only aim at some kinds of faults or problems, and they cannot evaluate the comprehensive risk of the power system. The risk of the power system comes from many aspects, and occurs with a certain probability. The reliability assessment method [14] can simulate all kinds of faults of power systems, and quantitatively evaluate the risk of the power grid from the probability and consequences of faults. Its reliability indexes can better reflect the comprehensive risk of the power system. However, the traditional reliability assessment method [15] is mainly used in power network planning, and all of the network topology information is needed when calculating the reliability index. Large-scale interconnected power grids are composed of regional power grids belonging to different power companies. Because of the scope of jurisdiction and interests, power companies are more concerned about the reliability of their own grids. In Reference [16], in order to improve the computational efficiency of the reliability index of the interconnected power system, the external network was replaced by a simplified equivalent model. However, the equivalent model used only considers the power generation output and the load of the external network, and it did not consider the network topology of the external network, and did not consider the voltage influence of the external network on the internal network. Therefore, direct current (DC) power flow can only be used for contingency analysis when calculating the reliability index. Compared with the contingency analysis based on alternating current (AC) power flow, there will be larger errors.

One of the challenges in the operational reliability assessment of the interconnected power system is to select a reasonably accurate static equivalent model to simplify the external network. The commonly used static equivalence models of external networks include Thevenin equivalence [17–19], Ward equivalence and its extended methods [20–22], and radial equivalent independent (REI) equivalence and its extended methods [23,24]. These equivalence methods only consider the consistency of power flow before and after equivalence, but ignore the consistency of sensitivity between variables before and after equivalence. However, as a key step of reliability assessment, contingency analysis requires sensitivity calculations for different component faults. In particular, the sensitivity analysis based on AC power flow not only considers the power constraint of the line, but also considers the voltage constraint of the bus, which can more accurately reflect the influence of component failure on the grid than the sensitivity analysis based on DC power flow [25]. In Reference [26], a sensitivity consistent static equivalent (SCSE) model was proposed, which can not only maintain the consistency of power flow before and after the equivalent, but also keep the

sensitivity relationship between variables before and after the equivalent. Replacing the external network with the SCSE model can maintain the accuracy when calculating the reliability index of the internal network. The SCSE model proposed in Reference [26] requires all accurate information of the external network, which is technically and commercially impossible for the operational reliability evaluation of the internal network. How to evaluate the SCSE model online in the case of information isolation is a key issue.

Large-scale interconnected power systems belong to different companies, and there are technical and commercial barriers to sharing grid topology information and operational data between power companies online. Because of line failure, load fluctuation, and temporary adjustments of the power generation plan, the operational risk of the system is constantly changing. Only by timely monitoring the operation of the external network under the condition of information isolation, combined with the real-time data of the internal network, can the operational reliability index of the system be calculated. In this way, the operator of the internal power grid can make a decision according to the reliability level of the power grid operation to deal with the risks that are brought by the external network to the internal network. Therefore, this paper proposes to use the boundary PMU measurement data to evaluate the SCSE model of the external network online. The change of the operation state of the external network is reflected in its equivalent model in real time, which affects the reliability of the internal network. The measurement equation of the SCSE model was deduced, and the least square model was established to estimate the parameters of the SCSE model. The algorithm flow for calculating the operational reliability index of the power grid is given. The method proposed in this paper can effectively perceive the operational risks of the external network and the internal network, and provide a reference for the operator to make decisions.

The contents of this paper are as follows: Section 2 introduces the SCSE model. Section 3 derives the measurement equation of the SCSE model with PMU, constructs the least square model, and gives the solution algorithm. Section 4 gives the calculation flow of the operational reliability assessment. Section 5 gives the example analysis. Section 6 gives the conclusion.

2. SCSE Model of the External Network

The power system is a complex nonlinear system. In order to ensure the accuracy of the reliability calculation, the static equivalent model of the external network of the interconnected power system needs to take into account the particularity of different components, and ensure that the sensitivity of the variables is unchanged before and after the equivalence. In the existing equivalent models, the SCSE model [26] not only has the advantage of the consistency of power flow before and after equivalence, but also has the advantage of consistency of sensitivity among variables. This consistency of sensitivity ensures the accuracy of contingency analysis in the reliability calculation, which is not available in other equivalent methods. Therefore, this paper uses the SCSE model to simplify the external network.

As shown in Figure 1, the interconnected power system can be divided into three parts, namely the external network, the internal network, and the boundary buses. External networks are networks that need to be replaced by SCSE models. The internal network is a network that focuses on its operational reliability, and all its data are available. The boundary buses connect the internal and external networks.
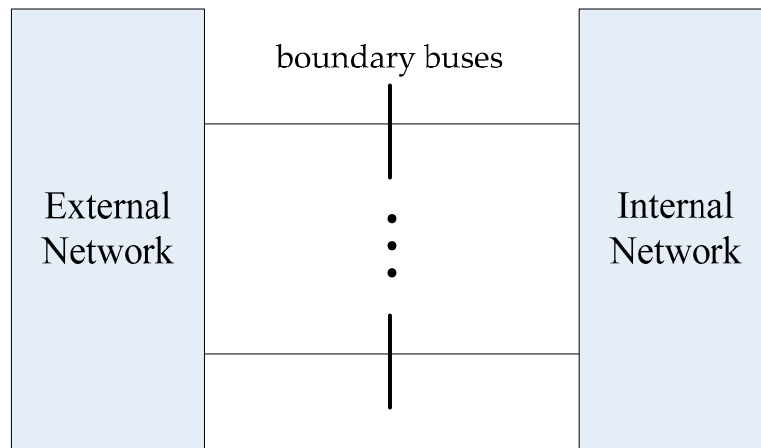
Figure 1. Interconnected power system.

The interconnected power system after the equivalent is shown in Figure 2. After the equivalent, all external buses are eliminated and replaced by the SCSE model, and the original topology of the internal network remains unchanged. The SCSE model of the external network is mainly composed of three kinds of variables, as follows:

- Admittance variables: y_{eqi} and y_{eqj} are the admittances of the equivalent branches between G_i and B_i, and between G_j and B_j, respectively. y_{eqij} and y_{eqGij} are the admittances of the equivalent branches between B_i and B_j, and between G_i and G_j, respectively. b_i and b_j are the susceptances of the equivalent grounding branches connected with the boundary buses B_i and B_j, respectively, where G_i and G_j are the generator buses, B_i and B_j are the boundary buses, $i, j = 1 \cdots N_B, i \neq j$, and N_B is the number of boundary buses.
- Voltage variable: $\dot{E}_i$ and $\dot{E}_j$ are the voltage phasors at the equivalent generator buses G_i and G_j, respectively.
- Power variables: S_{Li} and S_{Lj} are the equivalent loads at the boundary buses B_i and B_j, respectively. S_{eqGi} and S_{eqGj} are the equivalent generator output powers at G_i and G_j, respectively.
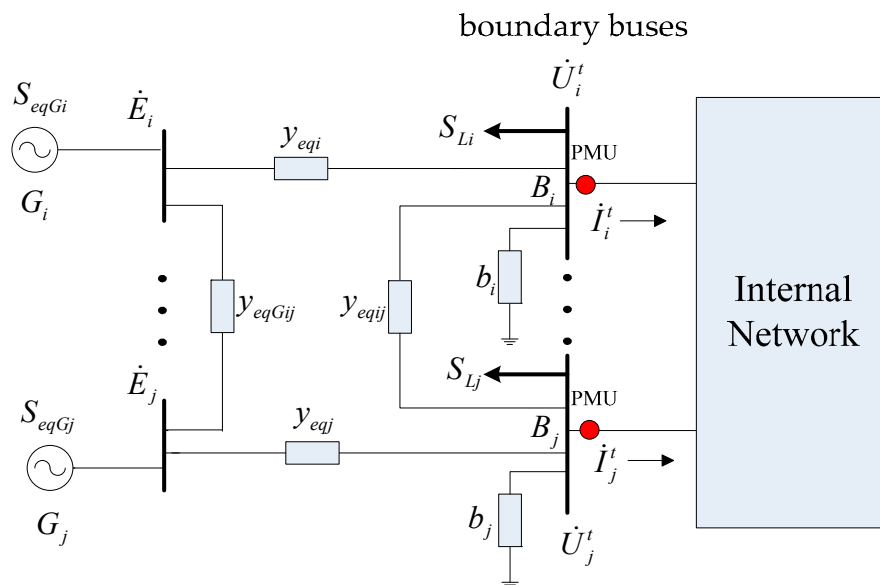

Figure 2. Interconnected power system after equivalence.

3. Online Update of the SCSE Model Based on Boundary PMU Measurement Data

Due to technical barriers and trade secrets, the actual topology and operational data of the network are difficult to share in real time among the power grids in different regions [27]. Due to the continuous changes in operation modes such as fault, maintenance, load fluctuation, and generator output adjustment, the internal network cannot obtain the SCSE model parameters of the external network in the case of information isolation, which is the main problem in assessing the operational reliability of the regional power grid of the interconnected power system. Since the network topology of the power grid does not change frequently in a short period of time, the load and generator output also change slowly, such that it can be assumed that the SCSE model parameters of the external network are constant values within a short period of time. The PMU can be used to measure the voltage and current of the boundary bus in real time during this period. The measurement equation of the external network equivalent parameter is derived from Kirchhoff's current law, and the least squares model is constructed to estimate the SCSE model parameters of the external network online. By updating the SCSE model of the external network according to the time period, the internal network can track the operational information of the external network online without accurate data of the external network. Then, the operational reliability index of the internal network can be evaluated by taking into account the impact of the external network on the internal network. It provides reference information for operators of the internal network to perceive grid risks and to make decisions in time.

3.1. Measurement Equations

In order to estimate the parameters of the equivalent model of the external network using the measured data of the boundary bus PMU, it is necessary to construct the measurement equation. As shown in Figure 2, the parameters to be estimated for the SCSE model are $x = \{\dot{E}_i, \dot{E}_j, y_{eqi}, y_{eqj}, y_{eqij}, y_{eqGij}, b_i, b_j, S_{Li}, S_{Lj}, S_{eqGi}, S_{eqGj}\}$. The boundary PMU measures the voltage and current of bus B_i as $\dot{U}_i^t$ and $\dot{I}_i^t$, and bus B_j as $\dot{U}_j^t$ and $\dot{I}_j^t$, respectively, where $i, j = 1 \cdots N_B$, $i \neq j$, N_B is the number of boundary buses, $t = 1, \cdots, M$, and M is the number of PMU samples in the given period of time. The following measurement equations can be derived from Kirchhoff's current law:

$$f_i^t(x) = (\dot{E}_i - \dot{U}_i^t)y_{eqi} - \dot{I}_i^t - \left(\frac{S_{Li}}{\dot{U}_i^t}\right)^* - b_i\dot{U}_i^t - \sum_{i=1,j\neq i}^{N_B}(U_i^t - U_j^t)y_{eqij} = 0; \tag{1}$$

$$g_i^t(x) = \left(\frac{S_{eqGi}}{\dot{E}_i}\right)^* - \sum_{i=1,i\neq j}^{N_B}(E_i - E_j)y_{eqGij} - (\dot{E}_i - \dot{U}_i^t)y_{eqi} = 0. \tag{2}$$

The complex variables in Equations (1) and (2) are respectively expanded according to the imaginary part and the real part, and Equations (3)–(6) are obtained as follows:

$$\begin{aligned}
f_{i(\text{Re})}^t(x) = {} & (\dot{E}_i - \dot{U}_i^t)_{\text{Re}}y_{eqi(\text{Re})}\left(\dot{U}_i^t\right)^*_{\text{Re}} + (\dot{E}_i - \dot{U}_i^t)_{\text{Im}}y_{eqi(\text{Im})}\left(\dot{U}_i^t\right)^*_{\text{Re}} \\
& + (\dot{E}_i - \dot{U}_i^t)_{\text{Re}}y_{eqi(\text{Im})}\left(\dot{U}_i^t\right)^*_{\text{Im}} + (\dot{E}_i - \dot{U}_i^t)_{\text{Im}}y_{eqi(\text{Re})}\left(\dot{U}_i^t\right)^*_{\text{Im}} - \left(\dot{U}_i^t\right)^*_{\text{Re}}\dot{I}_{i(\text{Re})}^t \\
& - \left(\dot{U}_i^t\right)^*_{\text{Im}}\dot{I}_{i(\text{Im})}^t - (S_{Li})^*_{\text{Re}} - \sum_{i=1,i\neq j}^{N_B}\left[(U_i^t - U_j^t)_{\text{Re}}y_{eqij(Re)}\left(\dot{U}_i^t\right)^*_{\text{Re}}\right. \\
& + (\dot{U}_i^t - \dot{U}_j^t)_{\text{Re}}y_{eqij(\text{Im})}\left(\dot{U}_i^t\right)^*_{\text{Im}} + (\dot{U}_i^t - \dot{U}_j^t)_{\text{Im}}y_{eqij(\text{Im})}\left(\dot{U}_i^t\right)^*_{\text{Re}} \\
& + \left.(\dot{U}_i^t - \dot{U}_j^t)_{\text{Im}}y_{eqij(\text{Re})}\left(\dot{U}_i^t\right)^*_{\text{Im}}\right] = 0
\end{aligned} \tag{3}$$

$$
\begin{aligned}
f^t_{i(\mathrm{Im})}(x) = {} & (\dot{E}_i - \dot{U}^t_i)_{\mathrm{Im}} y_{eqi(\mathrm{Re})} \left(\dot{U}^t_i\right)^*_{\mathrm{Re}} + (\dot{E}_i - \dot{U}^t_i)_{\mathrm{Im}} y_{eqi(\mathrm{Im})} \left(\dot{U}^t_i\right)^*_{\mathrm{Im}} \\
& + (\dot{E}_i - \dot{U}^t_i)_{\mathrm{Re}} y_{eqi(\mathrm{Re})} \left(\dot{U}^t_i\right)^*_{\mathrm{Im}} + (\dot{E}_i - \dot{U}^t_i)_{\mathrm{Re}} y_{eqi(\mathrm{Im})} \left(\dot{U}^t_i\right)^*_{\mathrm{Re}} - \left(\dot{U}^t_i\right)^*_{\mathrm{Re}} \dot{I}^t_{i(\mathrm{Im})} \\
& - \left(\dot{U}^t_i\right)^*_{\mathrm{Im}} \dot{I}^t_{i(\mathrm{Re})} - (S_{Li})^*_{\mathrm{Im}} - \sum_{i=1, i \neq j}^{N_B} \Bigg[(U^t_i - U^t_j)_{\mathrm{Re}} y_{eqij(\mathrm{Re})} \left(U^t_i\right)^*_{Im} \\
& + (\dot{U}^t_i - \dot{U}^t_j)_{\mathrm{Im}} y_{eqij(\mathrm{Im})} \left(\dot{U}^t_i\right)^*_{\mathrm{Im}} + (\dot{U}^t_i - \dot{U}^t_j)_{\mathrm{Re}} y_{eqij(\mathrm{Im})} \left(\dot{U}^t_i\right)^*_{\mathrm{Re}} \\
& + (\dot{U}^t_i - \dot{U}^t_j)_{\mathrm{Im}} y_{eqij(\mathrm{Re})} \left(\dot{U}^t_i\right)^*_{\mathrm{Re}} \Bigg] - b_i \dot{U}^t_i \left(\dot{U}^t_i\right)^* = 0
\end{aligned}
\tag{4}
$$

$$
\begin{aligned}
g^t_{i(\mathrm{Re})}(x) = {} & (S_{eqGi})^*_{\mathrm{Re}} - \sum_{i=1, i \neq j}^{N_B} \Bigg[(E_i - E_j)_{\mathrm{Re}} y_{eqGij(\mathrm{Re})} \left(E_i\right)^*_{Re} \\
& + (\dot{E}_i - \dot{E}_j)_{\mathrm{Re}} y_{eqGij(\mathrm{Im})} \left(\dot{E}_i\right)^*_{\mathrm{Im}} + (\dot{E}_i - \dot{E}_j)_{\mathrm{Im}} y_{eqGij(\mathrm{Im})} \left(\dot{E}_i\right)^*_{\mathrm{Re}} \\
& + (\dot{E}_i - \dot{E}_j)_{\mathrm{Im}} y_{eqGij(\mathrm{Re})} \left(\dot{E}_i\right)^*_{\mathrm{Im}} \Bigg] - (\dot{E}_i - \dot{U}^t_i)_{\mathrm{Re}} y_{eqi(\mathrm{Re})} \left(\dot{E}_i\right)^*_{\mathrm{Re}} \\
& - (\dot{E}_i - \dot{U}^t_i)_{\mathrm{Re}} y_{eqi(\mathrm{Im})} \left(\dot{E}_i\right)^*_{\mathrm{Im}} - (\dot{E}_i - \dot{U}^t_i)_{\mathrm{Im}} y_{eqi(\mathrm{Im})} \left(\dot{E}_i\right)^*_{\mathrm{Re}} \\
& - (\dot{E}_i - \dot{U}^t_i)_{\mathrm{Im}} y_{eqi(\mathrm{Re})} \left(\dot{E}_i\right)^*_{\mathrm{Im}} = 0
\end{aligned}
\tag{5}
$$

$$
\begin{aligned}
g^t_{i(\mathrm{Im})}(x) = {} & (S_{eqGi})^*_{\mathrm{Im}} - \sum_{i=1, i \neq j}^{N_B} \Bigg[(E_i - E_j)_{\mathrm{Im}} y_{eqGij(\mathrm{Re})} \left(E_i\right)^*_{Re} \\
& + (\dot{E}_i - \dot{E}_j)_{\mathrm{Im}} y_{eqGij(\mathrm{Im})} \left(\dot{E}_i\right)^*_{\mathrm{Im}} + (\dot{E}_i - \dot{E}_j)_{\mathrm{Re}} y_{eqGij(\mathrm{Im})} \left(\dot{E}_i\right)^*_{\mathrm{Re}} \\
& + (\dot{E}_i - \dot{E}_j)_{\mathrm{Re}} y_{eqGij(\mathrm{Re})} \left(\dot{E}_i\right)^*_{\mathrm{Im}} \Bigg] - (\dot{E}_i - \dot{U}^t_i)_{\mathrm{Im}} y_{eqi(\mathrm{Re})} \left(\dot{E}_i\right)^*_{\mathrm{Re}} \\
& - (\dot{E}_i - \dot{U}^t_i)_{\mathrm{Im}} y_{eqi(\mathrm{Im})} \left(\dot{E}_i\right)^*_{\mathrm{Im}} - (\dot{E}_i - \dot{U}^t_i)_{\mathrm{Re}} y_{eqi(\mathrm{Im})} \left(\dot{E}_i\right)^*_{\mathrm{Re}} \\
& - (\dot{E}_i - \dot{U}^t_i)_{\mathrm{Re}} y_{eqi(\mathrm{Re})} \left(\dot{E}_i\right)^*_{\mathrm{Im}} = 0
\end{aligned}
\tag{6}
$$

where $()^*$ denotes the conjugate operation. The subscripts $(*)_{\mathrm{Re}}$ and $(*)_{\mathrm{Im}}$ in Equations (3)–(6) respectively represent the real part and the imaginary parts of the complex variable $(*)$. $f^t_{i(\mathrm{Re})}(x)$, $f^t_{i(\mathrm{Im})}(x)$, $g^t_{i(\mathrm{Re})}(x)$, and $g^t_{i(\mathrm{Im})}(x)$ are the measurement equations separating the real and imaginary parts of Equations (1) and (2), respectively. Through the above measurement equation, with the inspecting data $\dot{U}^t_i$, $\dot{I}^t_i$, $\dot{U}^t_j$, and $\dot{I}^t_j$ of the boundary PMU, all the SCSE model parameters x of the external network can be estimated, where $x = \{\dot{E}_i, \dot{E}_j, y_{eqi}, y_{eqj}, y_{eqij}, y_{eqGij}, b_i, b_j, S_{Li}, S_{Lj}, S_{eqGi}, S_{eqGj}\}$.

3.2. Least Squares Model of the SCSE Model Parameters

Based on the measurement Equations (3)–(6), the least squares model of parameters of the SCSE model is constructed as shown in Equation (7).

$$
L = \min \left\{ \sum_{t=1}^{M} \sum_{i=1}^{N_B} \left[\left(f^t_{i(Re)}(x) \right)^2 + \left(f^t_{i(Im)}(x) \right)^2 + \left(g^t_{i(Re)}(x) \right)^2 + \left(g^t_{i(Im)}(x) \right)^2 \right] \right\}.
\tag{7}
$$

In order to ensure that the least squares model shown in Equation (7) has a sufficiently accurate solution, the number of measurement Equations (3)–(5) must be greater than the number of unknown parameters. From the equivalent model shown in Figure 2, we can see that the number of each parameter $\left(\dot{E}_i \right)_{\mathrm{Re}}$, $\left(\dot{E}_i \right)_{\mathrm{Im}}$, $(S_{eqGi})_{\mathrm{Re}}$, $(S_{eqGi})_{\mathrm{Im}}$, $(S_{Li})_{\mathrm{Re}}$, $(S_{Li})_{\mathrm{Im}}$, $y_{eqi(\mathrm{Re})}$, $y_{eqi(\mathrm{Im})}$, and b_i is N_B, and there are $9N_B$ unknown parameters together. The number of each parameter $y_{eqij(\mathrm{Re})}$, $y_{eqij(\mathrm{Im})}$, $y_{eqGij(\mathrm{Re})}$, and $y_{eqGij(\mathrm{Im})}$ is $N_B(N_B - 1)/2$, and there are $2N_B(N_B - 1)$ unknown parameters together. The number of measurement equations is $4MN_B$, which must satisfy the following inequality:

$$
4MN_B > 9N_B + 2N_B(N_B - 1).
\tag{8}
$$

After transformation, it can be obtained that

$$M > N_B/2 + 7/4. \tag{9}$$

It can be seen from Equation (9) that, when solving the SCSE model parameters of the external network using the least squares model shown in Equations (3)–(7), the sampling frequency M of PMU in each period must satisfy Equation (9). Since the least squares model is a nonlinear equation, the global optimization algorithm can be used to avoid falling into a local optimum [28], such that a more accurate sensitivity equivalent model can be obtained.

4. Operational Reliability Assessment Procedure of the Interconnected Regional Power Grid

The main difference between the operational reliability assessment and the traditional reliability assessment for planning is that the operational reliability assessment only calculates reliability indexes based on the current operational profile of the grid. The load model uses a single-point load at the current time, rather than a long-term load curve. The network topology and the equivalent model of the external network in the interconnected power grid all adopt the current value, so the calculated reliability index can reflect the actual operational risk of the power grid. The supervisory control and data acquisition (SCADA) system can support online acquisition of internal network data [29]. The steps of the operational reliability assessment of the interconnected power grid using boundary PMU measurement data to update the external network SCSE model online are as follows:

Step 1: The PMU is used to measure the voltage $\dot{U}_i^t$, $\dot{U}_j^t$, and current $\dot{I}_i^t$, $\dot{I}_j^t$ of the boundary bus. A total of M times were measured at equal time intervals over a set period of time.

Step 2: All PMU measurements in this time period are substituted into the measurement equation shown in Equations (3)–(6), and then the least squares model shown in Equation (7) is established.

Step 3: The global optimization algorithm is used to solve the least squares model shown in Equation (7), and the SCSE model of the external network in this period is obtained.

Step 4: The external network SCSE model of the time period is spliced with the internal network to form a network topology for calculating the operational reliability index of the internal network.

Step 5: The operation data of the internal network is extracted at the current moment, including the load of each bus and the output of each generator.

Step 6: A system state is selected using a Monte Carlo simulation. When evaluating the reliability index of the internal network in the interconnected power grid, the external network is replaced by the SCSE model, and it is assumed that the equivalent components in the external network do not have any faults. System operating states include the load status and the component status. For operational reliability assessments, the load is determined by the actual operation of the internal network. The load on each bus is a fixed value at the current moment, while the component state is simulated by a uniformly distributed random variable. Suppose that the probability of the down state of the kth component is p_k^{down}, and the probability of a derated state is $p_k^{derated}$. For the kth element, a uniformly distributed random number R_k is randomly selected in the [0, 1] interval, and the state of the component is determined by the position in the [0, 1] interval shown in Figure 3. If $p_k^{derated} + p_k^{down} < R_k \le 1$, the component is in the up state. If $p_k^{derated} < R_k \le p_k^{derated} + p_k^{down}$, the component is in the down state. If $0 \le R_k \le p_k^{derated}$, the component is in the derated state. The system state can be determined by sampling the states of all components in the internal network.
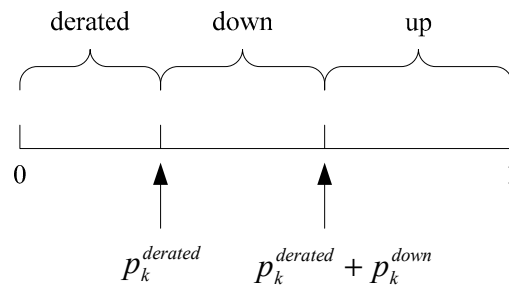
Figure 3. State sampling diagram of the *k*th component.

Step 7: The contingency analysis, based on a sensitivity technique with AC power flow, is implemented for the selected system state to identify if there is any overloading, voltage violation, isolated bus, or split island. Consider a case of the line *i–j* outage in a transmission system. Assume that the flows on the two ends of the line *i–j* before its outage are $P_{ij} + jQ_{ij}$ and $P_{ji} + jQ_{ji}$, and imagine that there are two additional power injections at the buses *i* and *j* in the pre-outage state, which are denoted by $\Delta P_i + j\Delta Q_i$ and $\Delta P_j + j\Delta Q_j$. If the additional power injections can produce power flow increments such that the power flows on the system are the same as those in the post-outage state, the effect of the additional power injections is completely equivalent to the outage of the line *i–j*. It can be proven that the power flows on the line *i–j* and the additional power injections in the pre-outage state have the following relationship [30]:

$$
\begin{bmatrix} P_{ij} \\ Q_{ij} \\ P_{ji} \\ Q_{ji} \end{bmatrix} = \left[\begin{bmatrix} 1 & 0 & 0 & 0 \\ 0 & 1 & 0 & 0 \\ 0 & 0 & 1 & 0 \\ 0 & 0 & 0 & 1 \end{bmatrix} - \begin{bmatrix} \frac{\partial P_{ij}}{\partial P_i} & \frac{\partial P_{ij}}{\partial Q_i} & \frac{\partial P_{ij}}{\partial P_j} & \frac{\partial P_{ij}}{\partial Q_j} \\ \frac{\partial Q_{ij}}{\partial P_i} & \frac{\partial Q_{ij}}{\partial Q_i} & \frac{\partial Q_{ij}}{\partial P_j} & \frac{\partial Q_{ij}}{\partial Q_j} \\ \frac{\partial P_{ji}}{\partial P_i} & \frac{\partial P_{ji}}{\partial Q_i} & \frac{\partial P_{ji}}{\partial P_j} & \frac{\partial P_{ji}}{\partial Q_j} \\ \frac{\partial Q_{ji}}{\partial P_i} & \frac{\partial Q_{ji}}{\partial Q_i} & \frac{\partial Q_{ji}}{\partial P_j} & \frac{\partial Q_{ji}}{\partial Q_j} \end{bmatrix} \right] \begin{bmatrix} \Delta P_i \\ \Delta Q_i \\ \Delta P_j \\ \Delta Q_j \end{bmatrix} . \tag{10}
$$

The additional power injections at the buses *i* and *j* can be obtained by solving Equation (10). Then, the increments of bus voltage magnitudes and angles due to the line *i–j* outage can be obtained by solving the following equation:

$$
[J] \begin{bmatrix} \Delta \delta \\ \Delta V / V \end{bmatrix} = [\Delta I], \tag{11}
$$

where $[J]$ is the Jacobian matrix of the power flow equations in the pre-outage state. $[\Delta V/V]$ is the voltage magnitude increment subvector, whose elements are $\Delta V_i/V_i$, $[\Delta \delta]$ is the voltage angle increment subvector, whose elements are δ_i, and $[\Delta I]$ is defined as shown in Equation (12).

$$
[\Delta I] = \left[0, \cdots, 0, \Delta P_i, 0, \cdots, 0, \Delta P_j, 0, \cdots, 0, \Delta Q_i, 0, \cdots, 0, \Delta Q_j, 0, \cdots, 0 \right]^T . \tag{12}
$$

Once the bus voltages are obtained, the line power flows following the line *i–j* outage can be calculated. A similar procedure can be applied to multiple line outages.

Step 8: When an outage causes system problems after the contingency analysis, generations should be rescheduled to alleviate constraint violations, and, at the same time, to avoid any load curtailment if possible, or to minimize the total load curtailment if unavoidable. The power generation adjustment measures after a fault are realized by solving the optimal power flow (OPF) [14], shown in Equations (13)–(20). The objective function of the OPF model is the minimization of the total load curtailment, whereas load curtailments at buses are the solutions of the model. If the load curtailment is not zero after the OPF, the selected system state is a failed one. Then, the system state and the load curtailment are recorded.

The objective function is shown in Equation (13):

$$\min \sum_{i \in ND} C_i, \tag{13}$$

and is subject to the following:

$$P_i - P_{load(i)} + C_i = 0 \quad i \in ND, \tag{14}$$

$$Q_i - Q_{load(i)} = 0 \quad i \in ND, \tag{15}$$

$$P_{G(i)}^{\min} \leq P_i \leq P_{G(i)}^{\max} \quad i \in NG, \tag{16}$$

$$Q_{G(i)}^{\min} \leq Q_i \leq Q_{G(i)}^{\max} \quad i \in NG, \tag{17}$$

$$0 \leq C_i \leq P_{load(i)} \quad i \in ND, \tag{18}$$

$$T_k \leq T_k^{\max} \quad k \in NL, \tag{19}$$

$$V_i^{\min} \leq V_i \leq V_i^{\max} \quad i \in NB, \tag{20}$$

where C_i is the load curtailment variable at bus i; P_i and Q_i are the real and reactive power injections at bus i; $P_{load(i)}$ and $Q_{load(i)}$ are the real and reactive loads at bus i; $P_{G(i)}^{\min}$, $P_{G(i)}^{\max}$, $Q_{G(i)}^{\min}$, and $Q_{G(i)}^{\max}$ are the lower and upper limits, respectively, of the real and reactive power injections at the generation bus i; T_k is the power flow on line k; $T_k^{\max}$ is the rating limit of line k; V_i is the bus i voltage magnitude; $V_i^{\min}$ and $V_i^{\max}$ are the lower and upper limits of the voltage magnitude at bus i; ND, NG, NB, and NL are, respectively, the sets of load buses, generator buses, all buses, and all circuits in the system.

Step 9: It is determined whether all system states are calculated. If the set number of sampling wis not completed, the workflow returns to step 6. If all samples are calculated, the reliability index of expected energy not supplied (EENS, KWh/period) is calculated as follows:

$$EENS = \sum_{s \in F} \frac{n(s)C(s)T}{N}, \tag{21}$$

where $n(s)$ is the number of states s occurring in the sampling, and $C(s)$ is the load curtailment (KW) in state s. T is the time interval of the operational reliability assessment, N is the total number of samples, and F is the set of all of the failure system states.

Step 10: The operational reliability index of the network is output during this period, and the workflow jumps to the first step to start the calculation of the next period.

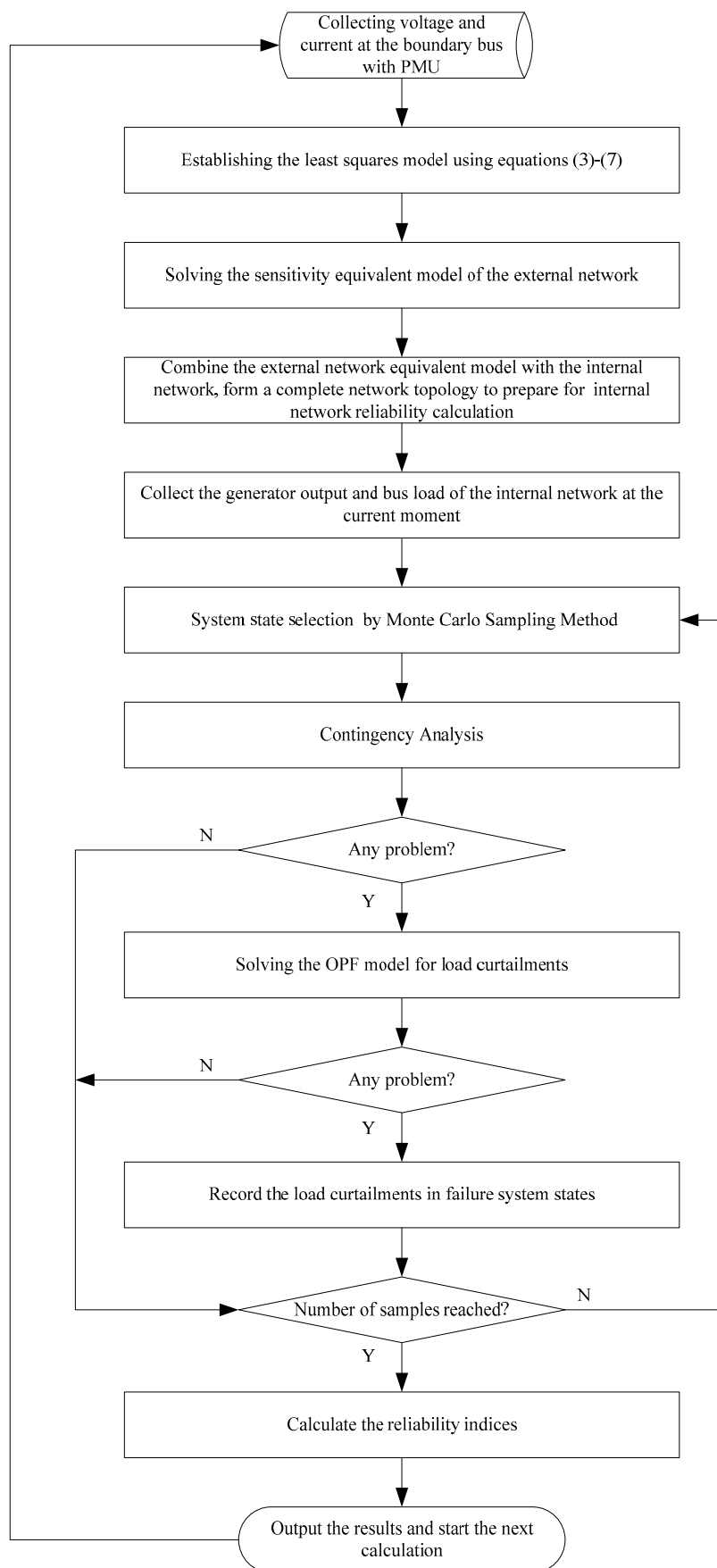The flow chart of the above process is shown in Figure 4.

Figure 4. Operational reliability evaluation flowchart.

5. Case Studies and Results

5.1. Test System Introduction

The proposed method was validated using the IEEE-RTS-96 test system [31]. The synchronous condenser located at the boundary bus 14 was out of operation, and the lines 16–19 were disconnected. The other data were identical with the original literature. The topology of the test system is shown in Figure 5, which was divided into the following: external network, boundary buses, and internal network.

External buses: 15–18, 21–22;

Boundary buses: 14, 24;

Internal buses: 1–13, 19–20, 23.

The PMU was installed at the boundary buses 14 and 24 near the internal network side for measuring the voltage of the boundary bus and the current flowing to the internal network. The interconnected network topology after the equivalent of the external network is shown in Figure 6. This test system has two boundary buses, such that it is necessary to estimate a total of 22 unknown variables online, which are $\left(\dot{E}_i\right)_{\mathrm{Re}}$, $\left(\dot{E}_i\right)_{\mathrm{Im}}$, $(S_{eqGi})_{\mathrm{Re}}$, $(S_{eqGi})_{\mathrm{Im}}$, $(S_{Li})_{\mathrm{Re}}$, $(S_{Li})_{\mathrm{Im}}$, $y_{eqi(\mathrm{Re})}$, $y_{eqi(\mathrm{Im})}$, b_i, $\left(\dot{E}_j\right)_{\mathrm{Re}}$, $\left(\dot{E}_j\right)_{\mathrm{Im}}$, $(S_{eqGj})_{\mathrm{Re}}$, $(S_{eqGj})_{\mathrm{Im}}$, $(S_{Lj})_{\mathrm{Re}}$, $(S_{Lj})_{\mathrm{Im}}$, $y_{eqj(\mathrm{Re})}$, $y_{eqj(\mathrm{Im})}$, b_j, $y_{eqij(\mathrm{Re})}$, $y_{eqij(\mathrm{Im})}$, $y_{eqGij(\mathrm{Re})}$, and $y_{eqGij(\mathrm{Im})}$.
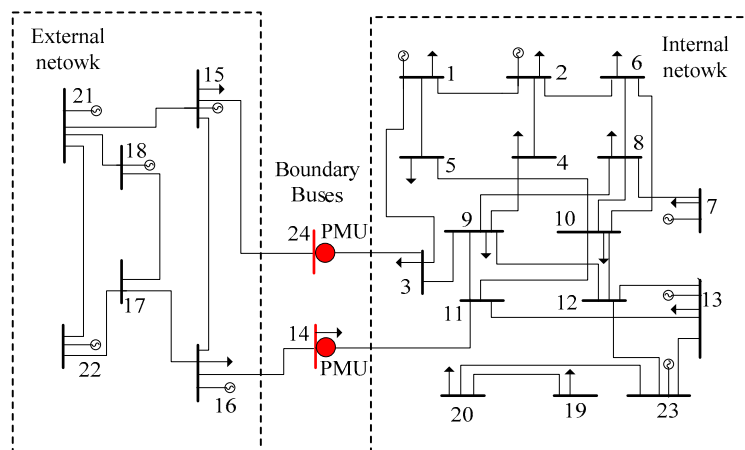

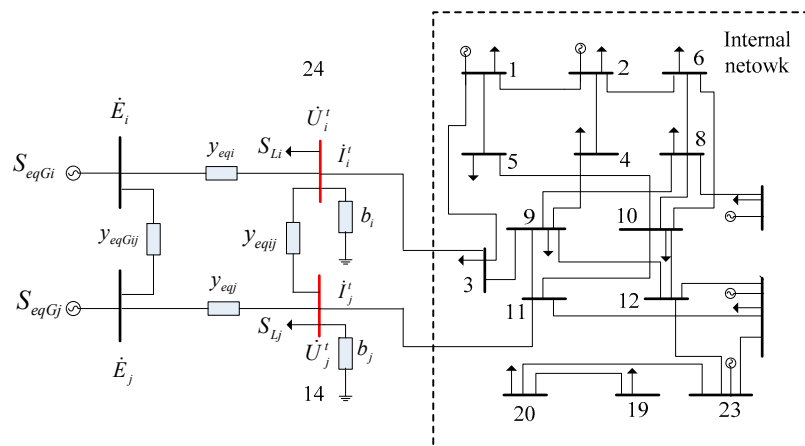**Figure 5.** Topology of the IEEE-RTS-96 test system.

Figure 6. Topology of the IEEE-RTS-96 test system after the equivalent.

5.2. Online Updating of the SCSE Model Based on PMU Measurement Data

The SCSE model of the external network could be estimated online through the measurement data of the boundary PMU. When the external network has a line failure, load fluctuation, or power output adjustment, it can be reflected in the SCSE model of the online update. The external network does not need to directly transfer data to the internal network, and the internal network can detect the changes of the external network. To verify the method proposed in this paper, 13 operating modes of the test system in Figure 5 were set as follows:

Case 1: Normal operation state, that is, the bus load is 100%, while there is no generator outage, and no line disconnection.

Case 2: The active load of the whole network is increased by 10%, while there is no generator outage, and no line disconnection.

Case 3: The reactive load of the whole network is increased by 10%, while there is no generator outage, and no line disconnection.

Case 4: The active and reactive load of the whole network is increased by 10%, while there is no generator outage, and no line disconnection.

Case 5: The active load of the whole network is reduced by 10%, while there is no generator outage, and no line disconnection.

Case 6: The reactive load of the whole network is reduced by 10%, while there is no generator outage, and no line disconnection.

Case 7: The active and reactive load of the whole network is reduced by 10%, while there is no generator outage, and no line disconnection.

Case 8: Lines 1–3, 2–6 of the internal network are disconnected. The load remains unchanged, and there is no generator outage.

Case 9: Bus 1 and Bus 2 of the internal network shut down a 20 MW generator. The load remains unchanged, and there is no generator outage.

Case 10: Bus 1 and Bus 2 of the internal network shut down a 20 MW generator. Lines 1–3 and line 2–6 are disconnected. The load remains unchanged.

Case 11: Lines 15–16, 15–21 of the external network are disconnected. The load remains unchanged, and there is no generator outage.

Case 12: Bus 15 of the external network shuts down a 155 MW generator. There is no generator outage, and no line disconnection.

Case 13: Bus 15 of the external network shuts down a 155 MW generator. Lines 15–21 of the external network are disconnected. The load remains unchanged.

The actual operation mode of a power grid is very complicated. The above 13 cases were set up from load increase, load decrease, line fault, generator fault, parameter change of external network, parameter change of internal network, and their combination. There were two boundary buses in the test system shown in Figure 5. Equation (9) shows that the number of PMU measurements must satisfy $M > 2.75$. Assuming that the system operational reliability assessment index is calculated every 10 min, within 10 min, the PMU needs to measure at least three sets of data to estimate all parameters of the SCSE model. In order to improve the accuracy of the parameter estimation, we set a time interval of two minutes for PMU measurement. PMU measured the voltage and current five times over 10 min. For the actual power system, the power grid did not remain unchanged in the time period, and each generator and each load point had small fluctuations, such that the data measured by the PMU were different. In order to make the IEEE-RTS-96 simulate the actual power grid operation to obtain reasonable boundary PMU measurement data, the load and generator output of the internal network were superimposed with a random variable to within 2% of its own amplitude. The actual values and estimated values of the external network equivalent model parameters of the 13 operating modes were calculated. The calculation results are shown in Figures 7–12.
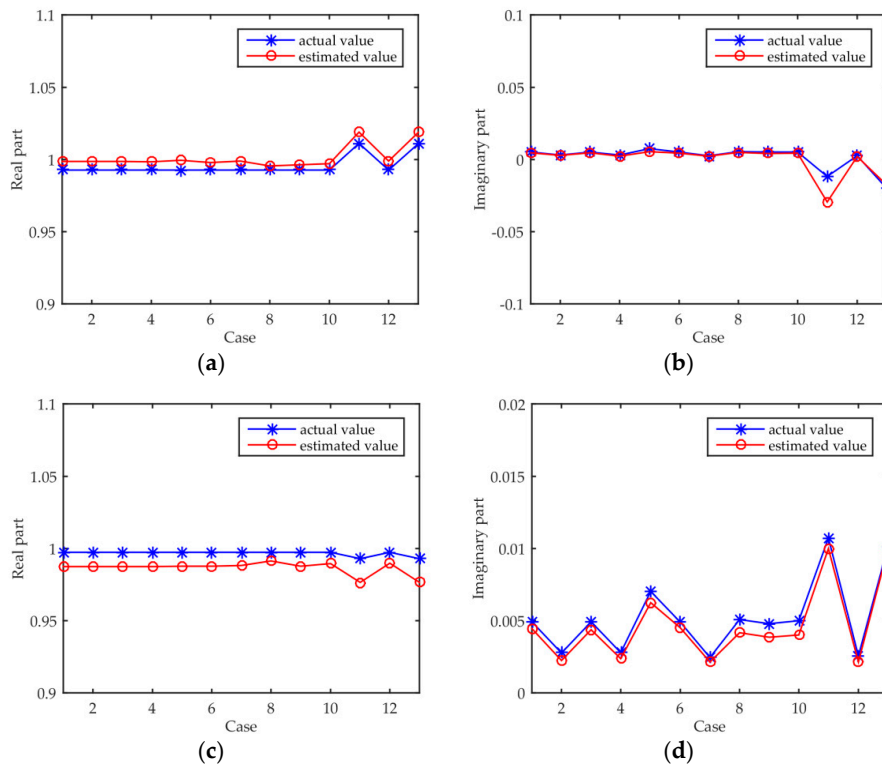
Figure 7. Voltage parameters of the sensitivity consistent static equivalent (SCSE) model. (**a**) $\left(\dot{E}_i\right)_{\text{Re}}$; (**b**) $\left(\dot{E}_i\right)_{\text{Im}}$; (**c**) $\left(\dot{E}_j\right)_{\text{Re}}$; (**d**) $\left(\dot{E}_j\right)_{\text{Im}}$.
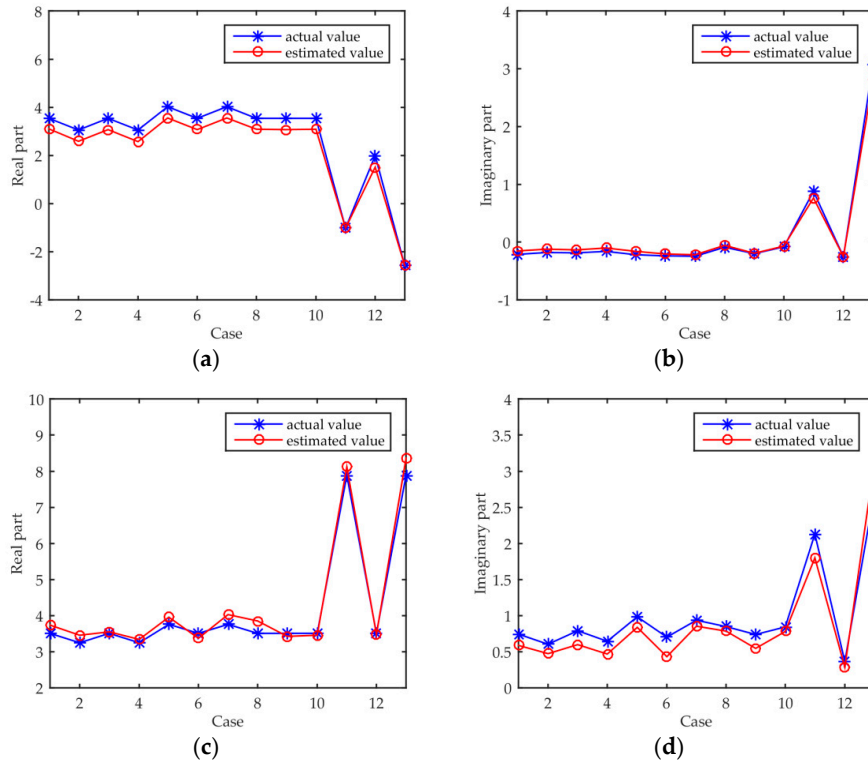
Figure 8. Generator output of the SCSE model. (**a**) $\left(S_{eqGi}\right)_{\text{Re}}$; (**b**) $\left(S_{eqGi}\right)_{\text{Im}}$; (**c**) $\left(S_{eqGj}\right)_{\text{Re}}$; (**d**) $\left(S_{eqGj}\right)_{\text{Im}}$.
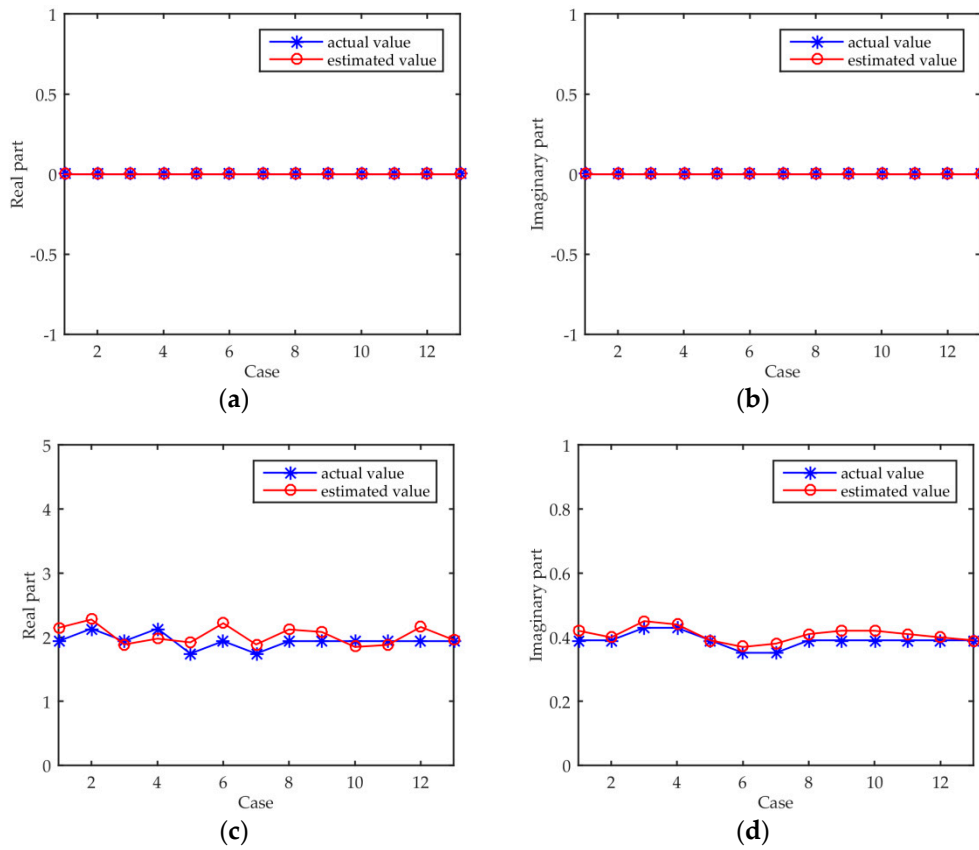
Figure 9. Load parameters of the SCSE model. (**a**) $(S_{Li})_{\mathrm{Re}}$; (**b**) $(S_{Li})_{\mathrm{Im}}$; (**c**) $\left(S_{Lj}\right)_{\mathrm{Re}}$; (**d**) $\left(S_{Lj}\right)_{\mathrm{Im}}$.
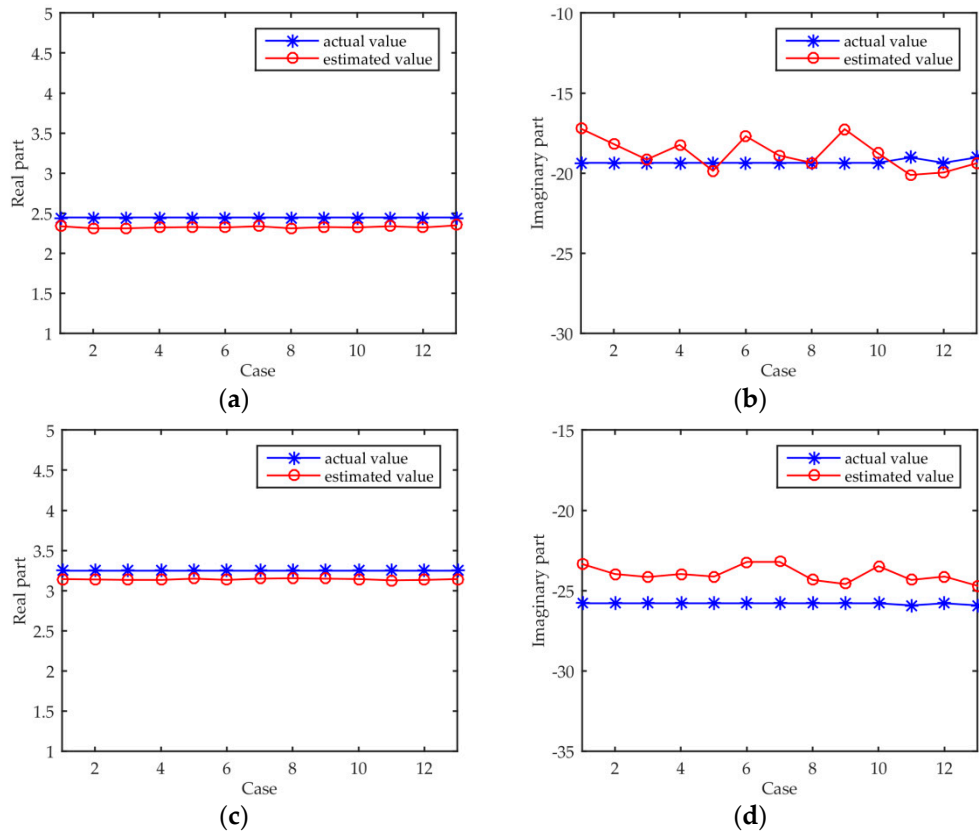
Figure 10. Admittance parameters of the SCSE model. (**a**) $y_{eqi(\mathrm{Re})}$; (**b**) $y_{eqi(\mathrm{Im})}$; (**c**) $y_{eqj(\mathrm{Re})}$; (**d**) $y_{eqj(\mathrm{Im})}$.
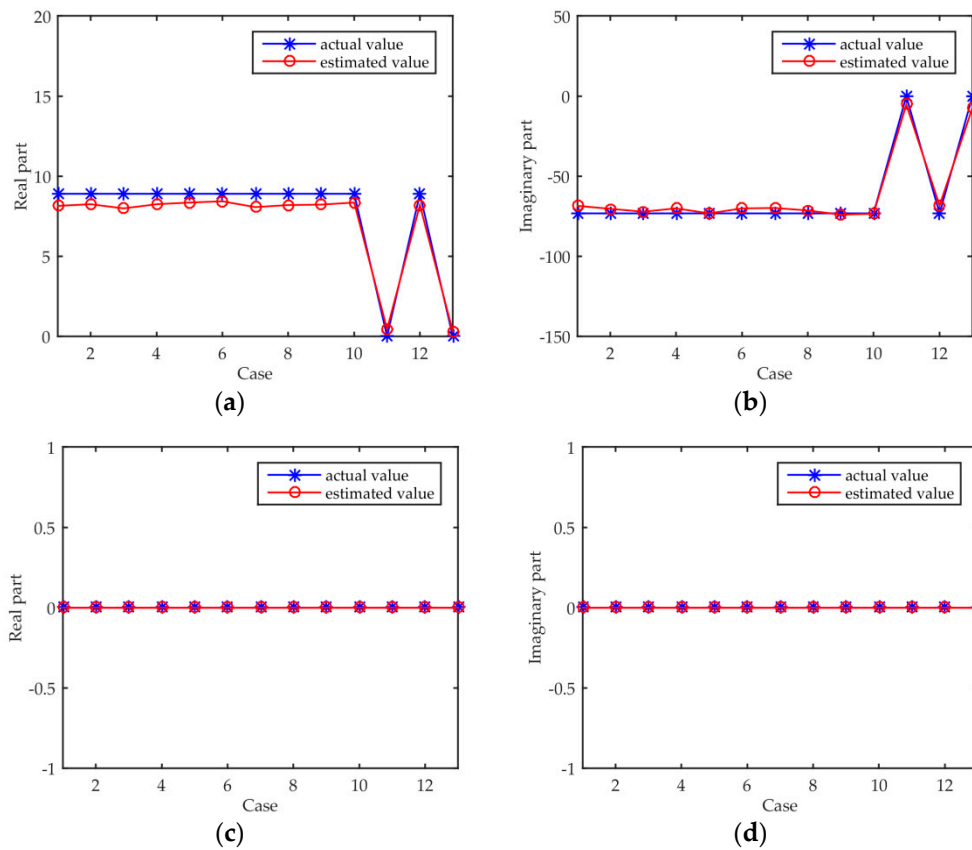
Figure 11. Admittance parameters of the SCSE model. (**a**) $y_{eqGij(\text{Re})}$; (**b**) $y_{eqGij(\text{Im})}$; (**c**) $y_{eqij(\text{Re})}$; (**d**) $y_{eqij(\text{Im})}$.
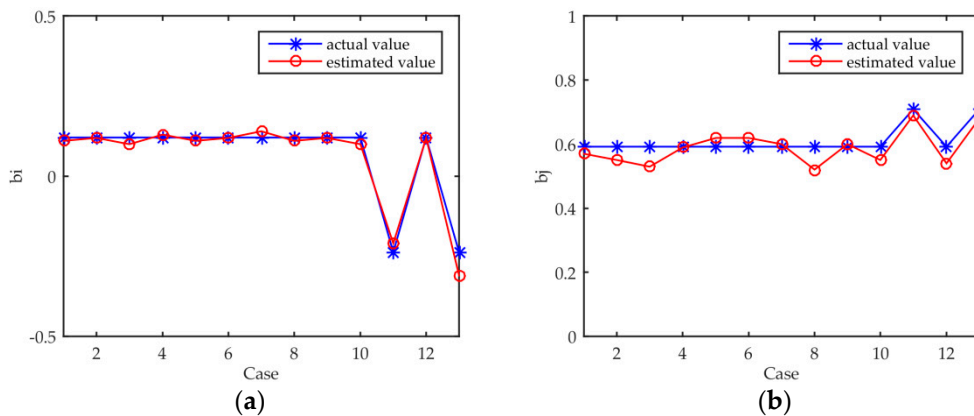

Figure 12. Susceptance parameters of the SCSE model. (**a**) b_i; (**b**) b_j.

5.3. Operational Reliability Assessment of the Interconnected Grid

With the updated SCSE model of the external network, the operational reliability index of the internal network can be calculated online. In order to verify the effectiveness and accuracy of the proposed method, three methods were used to calculate the reliability indexes of the internal network under 13 different operating conditions of the test system. The three methods were as follows:

Method 1: Both the internal network and the external network used the actual network topology. When calculating the operational reliability of the internal network, only the contingency analysis of the internal network was carried out, and no random failure of the external network components occurred.

Method 2: The transmission power between the internal network and the external network on the boundary bus was measured online. When calculating the reliability index of the internal network, the boundary bus was regarded as the PQ bus [32], and no random failure occurred.

Method 3: The method was as proposed in this paper. The SCSE model of the external network was updated online by using the boundary PMU measurement data. Then, it was combined with the actual internal network to form a simplified interconnected power system. The contingency analysis was only carried out for the internal network, and no random failure occurred for the external network equivalent model.

Method 1 was mainly used to verify the accuracy of Methods 2 and 3. The reliability calculation results of the three methods are shown in Figure 13 and Table 1. Figure 13a is the reliability index EENS of 13 operation modes using the three methods. Figure 13b shows the relative errors of Methods 2 and 3, using Method 1 as the standard. The relative error was defined as follows:

$$e = \frac{|EENS - EENS_{base}|}{EENS_{base}} \times 100\%. \tag{22}$$
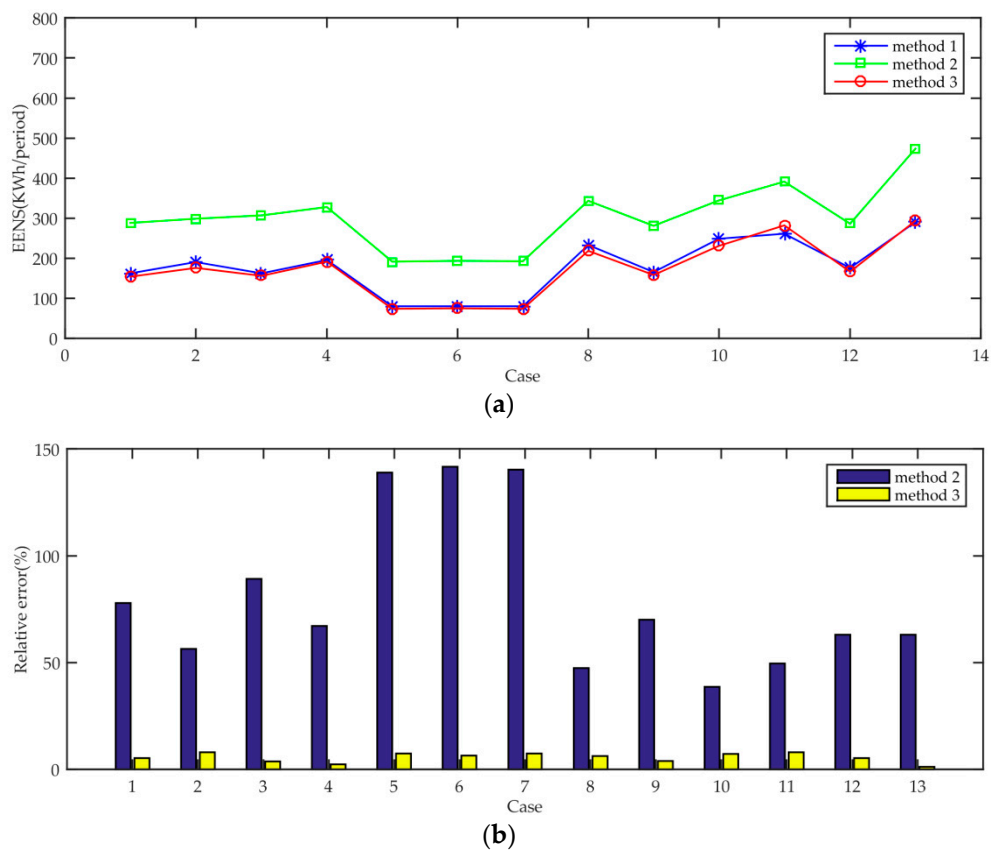

(a)

(b)

Figure 13. Calculation results of operational reliability. (**a**) Expected energy not supplied (EENS) of the three methods; (**b**) relative errors.

Table 1. Operational reliability index and relative error.

	Method 1	Method 2		Method 3	
	EENS (KWh/10 min)	EENS (KWh/10 min)	e (%)	EENS (KWh/10 min)	e (%)
Case 1	162.40	288.91	77.89	153.91	5.23
Case 2	190.85	298.62	56.47	175.65	7.96
Case 3	162.41	307.21	89.16	156.47	3.65
Case 4	196.10	327.64	67.08	191.63	2.28
Case 5	80.00	191.24	139.04	74.12	7.35
Case 6	80.21	193.78	141.60	74.98	6.51
Case 7	80.00	192.20	140.27	74.00	7.51
Case 8	233.19	343.82	47.44	218.74	6.20
Case 9	165.14	281.02	70.17	158.62	3.95
Case 10	248.88	344.98	38.62	230.93	7.21
Case 11	261.37	391.10	49.63	282.31	8.01
Case 12	175.76	286.73	63.13	166.37	5.35
Case 13	290.49	473.59	63.03	293.76	1.13

5.4. Discussion of Calculation Results

Case 1 was a benchmark case for normal operation, which was used for the comparative analysis of other cases. From Case 2 to Case 7, the active load and the reactive load of the system increased and decreased, respectively. The load change mainly affected the generator output parameters and the load parameters of the equivalent model, and did not affect the network topology. Therefore, the equivalent admittance of the external network would not be affected theoretically. From the results of Figures 7–12, it can be seen that the actual values of all admittance parameters from Case 2 to Case 7 remained unchanged, and only the generator output parameters and load parameters changed with the increase or decrease of the set load, and the voltage of the generator bus fluctuated slightly with the change of generator output, which is completely consistent with the theoretical analysis. Moreover, the results in the figures show that the data measured by the boundary PMU can estimate the parameters accurately.

Load changes had a significant impact on system reliability. It can be seen from the reliability calculation results in Figure 13 and Table 1 that, when the load increased, the EENS index was obviously improved, but the active load had a greater impact on the system reliability than the reactive load. This is because the definition of EENS is mainly aimed at the active load. The results of Case 8 show that, when the load was reduced by 10%, the EENS index rapidly reduced from 162.4 KWh/10 min to 80 KWh/10 min. The line had a larger running margin, due to the load drop. There are more kinds of remedial measures for faults. Therefore, the EENS index can be greatly reduced. From the results of Method 3, it can be seen that the external network equivalent model estimated by the boundary PMU was used to replace the accurate external network topology. With the system load changes, Method 3 could still track the operational reliability index with a relative error of up to 8%. Compared with the relative error of Method 2 of over 140%, the proposed method has higher accuracy and practical value.

When the network topology structure changes due to faults, maintenance, and other reasons, it has a significant impact on the reliability of the system. Cases 8–10 set three kinds of faults on the internal network, while the external network remained unchanged. From the results of Figures 7–12, it can be seen that the external network equivalent model did not change significantly, due to the failure of the internal network, except that the power and voltage fluctuated slightly with the change of the internal network. The reliability of the internal network was mainly affected by itself when the external network was unchanged. Case 8 disconnected lines 1–3 and 2–6, and EENS rose from 162.4 KWh/10 min to 233.19 KWh/10 min. In Case 9, bus 1 and bus 2 shut down a 20 MW generator. For the IEEE-RTS-96 test system, there were two 20 MW generators and two 76 MW generators on bus 1, and bus 2 was the same. Moreover, the power output of bus 1 and bus 2 was 172 MW, and the outage of a 20 MW generator would not significantly affect the reliability of the system. From the calculation

results in Table 1, it can be seen that the EENS of Case 9 was 165.14 KWh/10 min, which was little different from that of Case 1. For Case 10, the simultaneous outage of the generator and the line had a significant impact on system reliability, and EENS rose to 248.88 KWh/10 min. It can be seen from the calculation result of Method 3 in Table 1 that, when the internal network topology changed, the method proposed in this paper could accurately reflect the operational reliability of the internal network.

The reliability of the internal network in the interconnected power grid is affected by the external network. From Case 11 to Case 13, three kinds of faults were set in the external network, and the internal network remained unchanged. The change of the operation mode of the external network is reflected in its SCSE model. From the calculation results of Cases 11–13 in Figures 7–12, it can be seen that the admittance parameters of the equivalent model changed dramatically when an outage of the line occurred, and the power and voltage parameters of the equivalent model changed significantly when an outage of the generator occurred. These changes can be assessed online through the boundary PMU measurements. In this way, the internal network can perceive the risks from the external network, only depending on the boundary PMU measurements. The results of reliability calculation in Figure 13 and Table 1 show that the change of the operation mode of the external network was perceived by the boundary PMU, and was reflected in the impact on the reliability index EENS. In Case 11, the EENS of the internal network increased from 162.4 KWh/10 min to 261.37 KWh/10 min, due to the outage of lines 15–16 and 15–21 on the external network. For Case 12, the EENS of the internal network rose to 175.76 KWh/10 min, due to the outage of a 155 MW generator at bus 15. For Case 13, the EENS of the internal network rose to 290.49 KWh/10 min, due to the simultaneous outages of generators and lines. The results of Table 1 show that the error of the proposed method was significantly less than that of Method 2, and that Method 3 could more accurately perceive the risk of the external network to the internal network without relying on the actual information of the external network.

Table 1 shows the grid operational reliability results calculated by the three methods. Method 1 was based on the complete information of the internal network and the external network, but only the random failure of the internal network was considered for the calculation of the reliability index for the internal network. Method 2 only used the real-time power of the boundary buses to evaluate the reliability of the internal network. This method completely omitted the external network, and it is difficult to provide flexible remedial measures for the internal network in the process of a contingency analysis. The results would be significantly higher than the actual reliability index, and there would be greater errors. However, because this method can reflect the trend of the reliability index, and it does not depend on the information of external network, it is the most commonly used method at present. In Method 3, the boundary PMU was used to update the SCSE model of the external network online, and the reliability index of the internal network could be calculated online without depending on the actual information of the external network. The results show that the maximum relative error was about 8%, thereby proving it can accurately perceive the operational risks from the internal and external network, and provide an effective reference for decision-making by operators.

6. Conclusions

The main problem for the operation safety of a multi-region interconnected power system is how to evaluate the operation reliability index of each regional power network online under the conditions of information isolation. To solve this problem, the main conclusions of this paper are as follows:

- This paper proposes to replace the external network with the SCSE model, and to update the SCSE model online with boundary PMU, so as to evaluate the operational reliability of the internal network.
- Since the SCSE model has the advantage of consistent sensitivity among variables, the AC power flow method can be used to perform a contingency analysis in a reliability assessment with higher accuracy.

- The boundary PMU is used to update the external network SCSE model online, and the change of the operation mode of the external network can be perceived without depending on the actual information of the external network.
- The calculation flow of the operational reliability assessment for the interconnected power grid is given, which uses boundary PMU to update the SCSE model online in the case of information isolation.
- Three methods were used to calculate the 13 operation modes of the IEEE-RTS-96 test system. The results show that the proposed method could accurately calculate the operational reliability index only depending on the information of the internal network and the boundary measurement data, and provide an effective reference for operators in power grid decision-making.

Future works will mainly focus on error analysis, because the accuracy of operation reliability evaluation depends on the operation data error, PMU measurement error, equivalent model error, the influence of dynamic disturbance on steady-state calculation, reliability calculation error, and so on. In order to obtain reasonable and effective results, error analysis and control are very important.

Author Contributions: Conceptualization, D.Z., S.L., W.T., J.L. and C.F.; Methodology, D.Z., S.L., W.T., J.L. and C.F.; Software, D.Z., S.L., W.T., J.L. and C.F.; Validation, D.Z., S.L., W.T., J.L. and C.F.; Formal Analysis, D.Z., S.L., W.T., J.L. and C.F.; Investigation, D.Z., S.L., W.T., J.L. and C.F.; Resources, D.Z., S.L., W.T., J.L. and C.F.; Data Curation, D.Z., S.L., W.T., J.L. and C.F.; Writing-Original Draft Preparation, D.Z., S.L., W.T., J.L. and C.F.; Writing-Review & Editing, D.Z., S.L., W.T., J.L. and C.F.; Visualization, D.Z., S.L., W.T., J.L. and C.F.; Supervision, D.Z., S.L., W.T., J.L. and C.F.; Project Administration, D.Z., S.L., W.T., J.L. and C.F.; Funding Acquisition, D.Z., S.L., W.T., J.L. and C.F.

Conflicts of Interest: The authors declare no conflict of interest.

References

1. Huang, D.; Shu, Y.; Ruan, J.; Hu, Y. Ultra High Voltage Transmission in China. Developments, Current Status and Future Prospects. *Proc. IEEE* **2009**, *97*, 555–583. [CrossRef]
2. Biswas, S.; Nayak, P.K. State-of-the-art on the protection of FACTS compensated high-voltage transmission lines: A review. *High Volt.* **2018**, *3*, 21–30. [CrossRef]
3. Liu, S.; Li, J.; Wu, J.; Guo, T.; Jiang, L. Ultra-high voltage/extra-high voltage transmission-line protection based on longitudinal tapped impedance. *IET Gener. Transm. Distrib.* **2017**, *11*, 4158–4166. [CrossRef]
4. Rafique, S.F.; Shen, P.; Wang, Z.; Rafique, R.; Iqbal, T.; Ijaz, S.; Javaid, U. Global power grid interconnection for sustainable growth: Concept, project and research direction. *IET Gener. Transm. Distrib.* **2018**, *12*, 3114–3123. [CrossRef]
5. Liu, Z.; Chen, G.; Guan, X.; Wang, Q.; He, W. A concept discussion on northeast Asia power grid interconnection. *CSEE J. Power Energy Syst.* **2016**, *2*, 87–93. [CrossRef]
6. Zhang, F.; Xu, Z.; Jiao, B.; Yang, J.; Feng, J. Global energy interconnection based optimal power systems planning—A global perspective 2016–2050. In Proceedings of the 2017 China International Electrical and Energy Conference (CIEEC), Beijing, China, 25–27 October 2017; pp. 849–854.
7. Bialek, J.W. Why has it happened again? Comparison between the UCTE blackout in 2006 and the blackouts of 2003. In Proceedings of the 2007 IEEE Lausanne Power Tech, Lausanne, Switzerland, 1–5 July 2007; pp. 51–56.
8. Rahman, K.M.J.; Munnee, M.M.; Khan, S. Largest blackouts around the world: Trends and data analyses. In Proceedings of the 2016 IEEE International WIE Conference on Electrical and Computer Engineering (WIECON-ECE), Pune, India, 19–21 December 2016; pp. 155–159.
9. Wang, F.; Li, L.; Li, C.; Wu, Q.; Cao, Y.; Zhou, B.; Fang, B. Fractal Characteristics Analysis of Blackouts in Interconnected Power Grid. *IEEE Trans. Power Syst.* **2018**, *33*, 1085–1086. [CrossRef]
10. Chakraborty, N.C.; Banerji, A.; Biswas, S.K. Survey on major blackouts analysis and prevention methodologies. In Proceedings of the Michael Faraday IET International Summit 2015, Kolkata, India, 12–13 September 2015; pp. 297–302.

11. Guardado, R.A.; Guardado, J.L. A PMU Model for Wide-Area Protection in ATP/EMTP. *IEEE Trans. Power Deliv.* **2016**, *31*, 1953–1960. [CrossRef]

12. Kamwa, I.; Samantaray, S.R.; Joos, G. Compliance Analysis of PMU Algorithms and Devices for Wide-Area Stabilizing Control of Large Power Systems. *IEEE Trans. Power Syst.* **2013**, *28*, 1766–1778. [CrossRef]

13. Neyestanaki, M.K.; Ranjbar, A.M. An Adaptive PMU-Based Wide Area Backup Protection Scheme for Power Transmission Lines. *IEEE Trans. Smart Grid* **2015**, *6*, 1550–1559. [CrossRef]

14. Li, W. *Risk Assessment of Power Systems: Models, Methods, and Applications*, 2nd ed.; IEEE Press/Wiley: New York, NY, USA, 2014. [CrossRef]

15. Billinton, R.; Allan, R.N. *Reliability Evaluation of Power Systems*; Plenum: New York, NY, USA, 1996.

16. Zhang, W.; Billinton, R. Application of an adequacy equivalent method in bulk power system reliability evaluation. *IEEE Trans. Power Syst.* **1998**, *13*, 661–666. [CrossRef]

17. An, T.; Zhou, S.; Yu, J.; Zhang, Y. Tracking of Thevenin Equivalent Parameters on Weak Voltage Load Bus Groups. In Proceedings of the 2006 IEEE PES Power Systems Conference and Exposition, Atlanta, GA, USA, 29 October–1 November 2006; pp. 1570–1576.

18. Mou, X.; Li, W.; Li, Z. A preliminary study on the Thevenin equivalent impedance for power systems monitoring. In Proceedings of the 2011 4th International Conference on Electric Utility Deregulation and Restructuring and Power Technologies (DRPT), Weihai, China, 6–9 July 2011; pp. 730–733.

19. Tsai, S.S.; Wong, K. On-line estimation of thevenin equivalent with varying system states. In Proceedings of the 2008 IEEE Power and Energy Society General Meeting—Conversion and Delivery of Electrical Energy in the 21st Century, Pittsburgh, PA, USA, 20–24 July 2008; pp. 1–7.

20. Amerongen, R.A.M.V.; Meeteren, K.P.V. A Generalized Ward Equivalent for Security Analysis. *IEEE Power Eng. Rev.* **1982**, *PER-2*, 42–43. [CrossRef]

21. Deckmann, S.; Pizzolante, A.; Monticelli, A.; Stott, B.; Alsac, O. Studies on Power System Load Flow Equivalencing. *IEEE Trans. Power Appar. Syst.* **1980**, *PAS-99*, 2301–2310. [CrossRef]

22. Wu, F.F.; Monticelli, A. Critical review of external network modelling for online security analysis. *Int. J. Electr. Power Energy Syst.* **1983**, *5*, 222–235. [CrossRef]

23. Li, Z.; Yang, H. Application of REI Equivalent in Reactive Power Optimization Control in Regional Power Grid. In Proceedings of the 2011 Asia-Pacific Power and Energy Engineering Conference, Wuhan, China, 25–28 March 2011; pp. 1–4.

24. Neto, A.C.; Rodrigues, A.B.; Prada, R.B.; Silva, M.d.G.d. External Equivalent for Electric Power Distribution Networks with Radial Topology. *IEEE Trans. Power Syst.* **2008**, *23*, 889–895. [CrossRef]

25. Yu, J.; Zhang, M.; Li, W.; Yan, W.; Zhao, X. Sufficient and necessary condition of sensitivity consistency in static equivalent methods. *IET Gener. Transm. Distrib.* **2015**, *9*, 603–608. [CrossRef]

26. Yu, J.; Zhang, M.; Li, W.Y. Static Equivalent Method Based on Component Particularity Representation and Sensitivity Consistency. *IEEE Trans. Power Syst.* **2014**, *29*, 2400–2408. [CrossRef]

27. Yu, J.; Dai, W.; Li, W.; Liu, X.; Liu, J. Optimal Reactive Power Flow of Interconnected Power System Based on Static Equivalent Method Using Border PMU Measurements. *IEEE Trans. Power Syst.* **2018**, *33*, 421–429. [CrossRef]

28. Ugray, Z.; Lasdon, L.; Plummer, J.; Glover, F.; Kelly, J.; Marti, R. Scatter search and local NLP solvers: A multistart framework for global optimization. *INFORMS J. Comput.* **2007**, *19*, 328–340. [CrossRef]

29. Wu, J.; Cheng, Y.; Schulz, N.N. Overview of real-time database management system design for power system SCADA system. In Proceedings of the IEEE SoutheastCon 2006, Memphis, TN, USA, 31 March–2 April 2006; pp. 62–66.

30. Billinton, R.; Li, W. *Reliability Assessment of Electric Power Systems Using Monte Carlo Methods*; Plenum Press: New York, NY, USA; London, UK, 1994.

31. Grigg, C.; Wong, P.; Albrecht, P.; Allan, R.; Bhavaraju, M.; Billinton, R.; Chen, Q.; Fong, C.; Haddad, S.; Kuruganty, S.; et al. The IEEE Reliability Test System-1996. A report prepared by the Reliability Test System Task Force of the Application of Probability Methods Subcommittee. *IEEE Trans. Power Syst.* **1999**, *14*, 1010–1020. [CrossRef]
32. Görner, K.; Rehtanz, C.; Kolosok, I.N.; Korkina, E.; Glazunova, A.; Voropai, N.I.; Mutule; Brinkis, K.; Kochukov, O. Coordinated monitoring of large scale interconnected power systems. In Proceedings of the 2013 IEEE Power & Energy Society General Meeting, Vancouver, BC, Canada, 21–25 July 2013; pp. 1–5.